Optical Properties of Eu-Doped and Eu−Gd Co-Doped $CsMgCl_3$: Temperature Dependence of Rate Constants for $^5D_2$ and $^5D_1$ Cross Relaxation in Symmetric Eu(III)−Eu(III) Pairs

Ling Shi Xiao, Matthew Lang, and P. Stanley May*

Department of Chemistry, University of South Dakota, Vermillion, South Dakota 57069

Received: August 24, 1999; In Final Form: November 6, 1999

The luminescence properties of Eu in Eu-doped and Eu−Gd co-doped $CsMgCl_3$ are reported. Emission is observed from Eu^{2+}, Eu^{3+} in symmetric pairs and Eu^{3+} in what appears to be higher-order "clusters" of lanthanide ions. Rate constants for cross relaxation out of $^5D_1$ and $^5D_2$ are reported over the temperature ranges of 10−373 K and 10−298 K, respectively, for the symmetric Eu−Eu pair. The branching of $^5D_2$ cross relaxation between $^5D_2 \rightarrow {}^5D_1$ and $^5D_2 \rightarrow {}^5D_0$ is also reported.

1. Introduction

We are interested currently in energy transfer processes occurring within isolated pairs of lanthanide ions in the $CsMX_3$ halides $CsMgCl_3$, $CsCdBr_3$, and $CsMgBr_3$. These compounds adopt the hexagonal $CsNiCl_3$ structure of the space group $P6_3/mmc$, in which the halide ions form infinite chains of face-sharing octahedra running parallel to the c_3 crystal axis. The divalent ions reside at the centers of the octahedra and the Cs^+ ions lie between the infinite chains. The $[MX_6]^{4-}$ octahedra are slightly elongated along the c_3 axis so that the site symmetry of the divalent ion is D_{3d}. Trivalent lanthanides are known to enter these lattices predominately as a single type of pair, Ln^{3+}−(M^{2+} vacancy)−Ln^{3+}, with each pair substituting for three M^{2+} ions.[1,2] The lanthanides in the symmetric pair collapse slightly toward the M^{2+} vacancy, lowering their site symmetry to C_{3v}.

The main advantage to studying energy transfer in these systems is that they permit facile determination of the microscopic rate constants for the transfer of electronic energy between ions in specific, well-defined sites. Determination of the transfer rate constants is greatly simplified because there is only one type of transfer event, as opposed to the distribution of events which would be observed in a system with randomly distributed donors and acceptors. For the latter types of hosts, pairwise transfer rate constants cannot be determined directly from the luminescence characteristics of the donor and acceptor.

Optical investigations of Ln^{3+} ions in one or more of the $CsMX_3$ hosts include singly doped Pr^{3+},[3−6] Nd^{3+},[7−10] Tb^{3+},[11−13] Ho^{3+},[14,15] Eu^{3+},[16] Er^{3+},[17−24] Tm^{3+},[25] and Ce^{3+}[26] systems and co-doped Tm^{3+}−Pr^{3+},[27] Tm^{3+}−Ho^{3+},[28] Yb^{3+}−Er^{3+},[29] Gd^{3+}−Er^{3+},[30] and Ce^{3+}−Tm^{3+} [31] systems. By far, the majority of these spectroscopic investigations of lanthanide pairs in these hosts have centered on upconversion processes, especially in Er^{3+}:$CsCdBr_3$, wherein pair luminescence can be obtained at wavelengths shorter than the excitation wavelength(s).

In this paper, we report the optical properties of Eu-doped and Eu−Gd codoped $CsMgCl_3$. Our main emphasis is on the luminescence properties of Eu^{3+} in symmetric pairs leading to the determination of the pairwise rate constants for cross relaxation out of the $^5D_1$ and $^5D_2$ states. Rate constants for cross relaxation out of $^5D_1$ and $^5D_2$ are reported over the temperature ranges of 10−373 K and 10−298 K, respectively. The partitioning of $^5D_2$ cross relaxation between $^5D_2 \rightarrow {}^5D_1$ and $^5D_2 \rightarrow {}^5D_0$ is also reported. In addition to emission from Eu^{3+} in symmetric pairs, we observe emission due to Eu^{2+} and from Eu^{3+} in "clusters" which appear to consist of at least three lanthanide ions.

2. Experimental Section

$CsMgCl_3$ was prepared by fusing equimolar amounts of anhydrous CsCl and $MgCl_2$ under vacuum. The resulting samples were then sealed under vacuum in 9 mm Vycor ampules, and single crystals were grown from melt via the Bridgman method. Portions of the crystal boules with the highest optical quality were then selected, combined with the appropriate anhydrous lanthanide chloride(s), sealed under vacuum, and returned to the Bridgman furnace.

High-resolution luminescence spectra and time-dependent luminescence data were acquired using a PC-controlled, open-architecture system consisting of nitrogen laser/dye laser excitation (Laser Photonics models UV-12 and DL-14, respectively), a 0.46 M flat-field monochromator (Jobin-Yvon HR460), and a time-resolved photon-counting detection system consisting of a fast, red-sensitive, side-window photomultiplier (Hamamatsu R2949) and a multichannel scaler (Stanford Research SR430). The spectroscopic properties of Eu^{2+} were characterized using a SPEX Fluoromax photon counting spectrophotometer. For temperature dependence measurements, samples were attached to a copper mount in the sample compartment of a closed-cycle cryostat (CRYOMECH model ST15) using copper grease and indium foil.

3. Results and Discussion

3.1 Optical Properties of Eu^{2+} in $CsMgCl_3$. Upon UV excitation, all Eu-doped samples exhibit bright, pale-blue emission due to a broad band luminescence centered at ∼483 nm. We attribute this emission to Eu^{2+} ions, consistent with the observation of Eu^{2+} emission (albeit weak) at 476 nm in Eu-doped $CsCdBr_3$.[16] The excitation spectrum we observe for Eu^{2+} in $CsMgCl_3$ is also very similar in gross features to the $4f^7(^8S_{7/2}) \rightarrow 4f^65d^1(t_{2g})$ absorption region reported for Eu^{2+} in

* Corresponding author. E-mail: smay@usd.edu. Fax: (605) 677-6397.

10.1021/jp993003a CCC: $19.00
Published on Web 12/22/1999

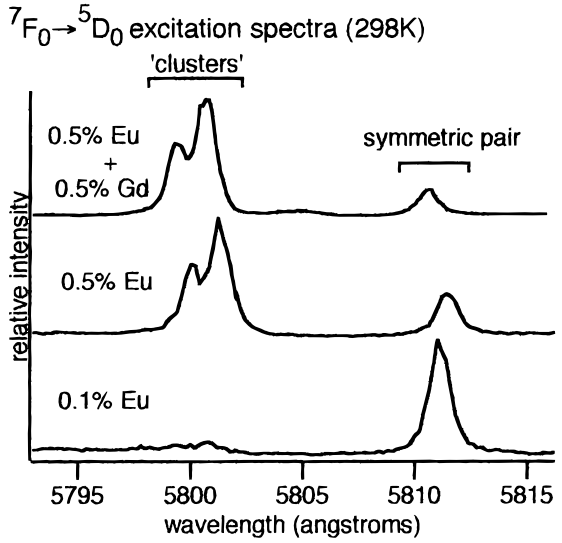

Figure 1. $^7F_0 \rightarrow {}^5D_0$ excitation spectra of 0.5% Eu (middle), 0.5% Eu/0.5% Gd (top), and 0.1% Eu (bottom) doped $CsMgCl_3$ at 298 K. These spectra were obtained by setting the spectrograph to zeroth order and filtering excitation light with a 610 nm low-pass filter, such that all luminescent Eu^{3+} sites were detected.

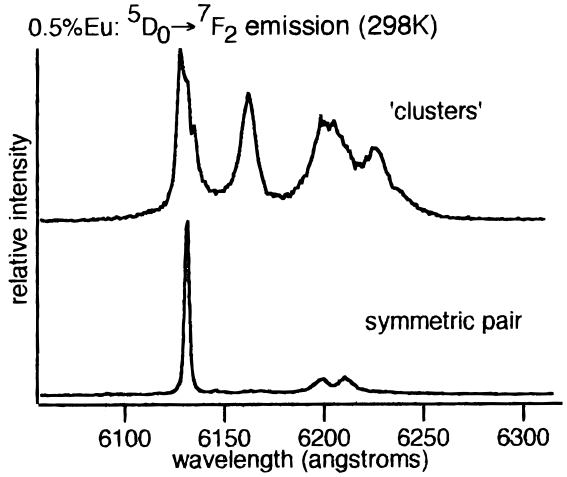

Figure 2. $^5D_0 \rightarrow {}^7F_2$ emission spectra of Eu^{3+} at 298 K in (top) clusters, obtained by exciting the $^7F_0 \rightarrow {}^5D_0$ band at 5801 Å and (bottom) symmetric pairs, obtained bythe exciting $^7F_0 \rightarrow {}^5D_0$ band at 5811 Å.

$CsCdBr_3$. Several of our samples also exhibit other broad luminescence bands blue-shifted relative to the 484 nm band, but none of these were common to all samples. At least some of these bands are probably also due to Eu^{2+} in other lattice sites. On the basis of its commonality to all samples and the similarity of its energy levels to that seen in $CsCdBr_3$, we attribute the 483 nm band to Eu^{2+} ions in normal Mg^{2+} lattice sites.

In contrast to its behavior in $CsCdBr_3$, Eu^{2+} appears to be a very efficient luminophor in $CsMgCl_3$, even at room temperature. Excitation into the $4f^7(^8S_{7/2}) \rightarrow 4f^65d^1(t_{2g})$ region from ~330−450 nm results in intense Eu^{2+} emission which overwhelms Eu^{3+} emission. In $CsCdBr_3$, excitation into Eu^{2+} absorption bands results predominately in Eu^{3+} emission.[16] This is in spite of the fact that the Eu^{2+}/Eu^{3+} ratio in $CsCdBr_3$ is almost certainly higher relative to that in $CsMgCl_3$, in which a significant percentage of Eu exists as Eu^{3+} (see section 3.6). Visual side-by-side comparison of 0.5% Eu:$CsMgCl_3$ and 0.5% Eu:$CsCdBr_3$ samples at room temperature under a hand-held UV lamp shows intense blue emission from 0.5% Eu:$CsMgCl_3$, but no detectable emission of any color from 0.5% Eu:$CsCdBr_3$.[32]

3.2. Optical Properties of Eu^{3+} in $CsMgCl_3$. In addition to Eu^{2+} emission, luminescence from at least three spectroscopically distinct Eu^{3+} sites is observed. Figure 1 shows $^7F_0 \rightarrow {}^5D_0$ excitation spectra (298 K) for samples nominally doped with 0.5% Eu + 0.5% Gd, 0.5% Eu, and 0.1% Eu. These spectra were obtained by setting the spectrograph to zeroth order and filtering excitation light with a 610 nm low-pass filter, such that all luminescent Eu^{3+} sites were detected. Three peaks are clearly observable in samples with 0.5% Eu, corresponding to three distinct Eu^{3+} sites, while only one well-defined peak is seen in the 0.1% Eu sample. For reasons outlined below, we assign the peak at 5811 Å to the symmetric Eu−vac−Eu pair and the two closely spaced peaks at 5800 and 5801 Å to strongly coupled Eu^{3+} ions in higher-order clusters.

Figure 2 shows the room-temperature $^5D_0 \rightarrow {}^7F_2$ emission spectra of the 0.5% Eu sample obtained via selective excitation into the three $^7F_0 \rightarrow {}^5D_0$ bands in Figure 1. The lower spectrum was obtained using 5811 Å excitation, the upper using 5801 Å excitation. Excitation into *either* of the two closely spaced "cluster" bands at 5800 and 5801 Å results in identical spectra with identical emission decay constants, indicating rapid exchange of energy between the Eu^{3+} ions corresponding to these two $^7F_0 \rightarrow {}^5D_0$ bands. The $^5D_0$ decay constant for the cluster emission is 1.0×10^4 s^{-1} at 298 K, dropping to ~1300 s^{-1} at 10 K.

Excitation into either of the $^7F_0 \rightarrow {}^5D_0$ cluster bands in the 0.5% Eu + 0.5% Gd sample also results in identical emission spectra with identical emission decay constants. However, in this case, the $^5D_0$ decay constant is only ~1300 s^{-1} at room temperature, less than one-seventh the value measured for the 0.5% Eu sample. The implication is that incorporation of Gd^{3+} ions in the clusters disrupts the quenching of $^5D_0$ emission, but does not affect rapid energy exchange between the Eu^{3+} ions in the cluster. As discussed in section 3.3, this behavior can be rationalized in terms of clusters consisting of at least three Ln^{3+} ions. Finally, we note that the $^5D_0$ decay constant for emission from the symmetrical pair is ~950 s^{-1} in all three samples, indicating that Gd^{3+} has no effect on $^5D_0$ relaxation in the symmetrical pair.

Figure 3 shows $^7F_0 \rightarrow {}^5D_1$ excitation spectra (298 K) for the same samples as in Figure 1. These spectra were obtained by setting the spectrograph to zeroth order and filtering excitation light with a 570 nm low-pass filter. Excitation into any of the peaks marked as "clusters" gives the same $^5D_0 \rightarrow {}^7F_2$ emission marked as "clusters" in Figure 2, even in the 0.5% Eu + 0.5% Gd sample, but does *not* result in $^5D_1$ emission. Excitation into the "symmetric pair" bands yields the same $^5D_0 \rightarrow {}^7F_2$ emission shown in Figure 2 for symmetric pairs and also results in emission from $^5D_1$. Note that, since a single Eu^{3+} can have no more than three peaks in this region, the presence of at least four (or more) "cluster" peaks associated with identical emission spectra reinforces our interpretation of at least two Eu^{3+} ions which are strongly coupled but occupy different lattice sites. Additionally, the fact that all $^7F_0 \rightarrow {}^5D_1$ cluster bands yield the same emission spectrum for the Eu−Gd co-doped sample suggests the presence of more than two ions in the cluster. If the cluster consisted of only two ions, then two distinct asymmetric Eu−Gd pairs would be present and one would expect at least some degree of selectivity between the pairs.

Comparison of the time dependence of $^5D_1$ emission for the symmetric pair in the Eu-doped and the Eu−Gd co-doped samples demonstrates that the emission we have attributed to

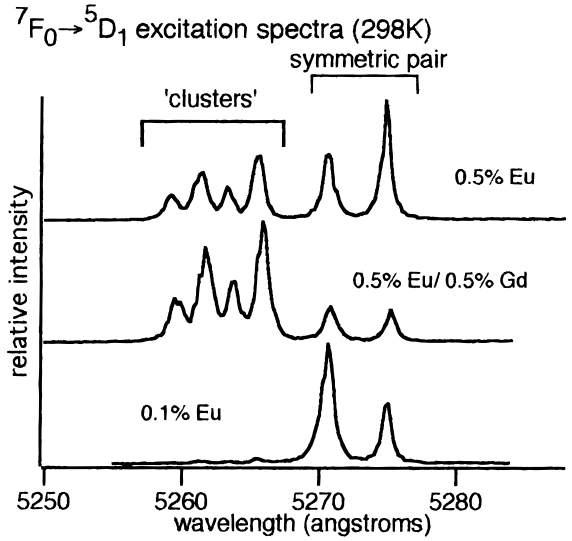

Figure 3. $^7F_0 \rightarrow {}^5D_1$ excitation spectra of 0.5% Eu (top), 0.5% Eu/ 0.5% Gd (middle), and 0.1% Eu (bottom) doped $CsMgCl_3$ at 298 K. These spectra were obtained by setting the spectrograph to zeroth order and filtering excitation light with a 570 nm low-pass filter, such that all luminescent Eu^{3+} sites were detected.

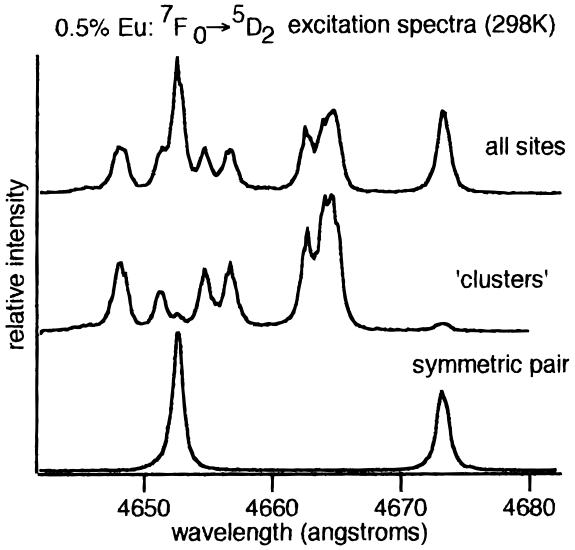

Figure 4. $^7F_0 \rightarrow {}^5D_2$ excitation spectra of 0.5% Eu:$CsMgCl_3$ at 298 K. Top spectrum obtained by setting the spectrograph to zeroth order and filtering excitation light with a 590 nm low-pass filter, such that all luminescent Eu^{3+} sites were detected. Middle spectrum obtained by monitoring $^5D_0 \rightarrow {}^7F_2$ cluster emission at 6162 Å. Bottom spectrum obtained by monitoring $^5D_1 \rightarrow {}^7F_1$ symmetric pair emission at 5380 Å.

symmetric pairs actually is from pairs and not from single ions. In the Eu-doped samples, room-temperature $^5D_1$ decay constants are 3660 s^{-1}. In the Eu−Gd co-doped samples, $^5D_1$ emission following pulsed excitation shows two components: a shorter-lived component with a decay constant identical to that obtained for Eu-doped samples and a longer-lived component with a decay constant of 1040 s^{-1}. Clearly, the Eu^{3+} ions responsible for this emission are paired with another Ln^{3+} ion in an identical chemical environment. The two decay constants for $^5D_1$ emission in Eu−Gd codoped samples are attributable to the presence of both Eu−vac−Eu and Eu−vac−Gd pairs, the larger decay constant being associated with the Eu−vac−Eu pair due to partial quenching via cross relaxation (see section 3.5).

$^7F_0 \rightarrow {}^5D_2$ excitation spectra (298 K) for the symmetric pair and for the clusters are shown in Figure 4 for the 0.5% Eu sample. The upper spectrum was obtained by setting the spectrograph to zeroth order and filtering excitation light with a 590 nm low-pass filter. The middle spectrum shows the cluster spectrum and was obtained by monitoring the $^5D_0 \rightarrow {}^7F_2$ emission of clusters at 6162 Å. No $^5D_1$ or $^5D_2$ emission from clusters is seen at room temperature, but relatively weak $^5D_1$ emission is seen at 10 K (decay constant = 11 600 s^{-1}). The lower spectrum is for the symmetric pairs and was obtained by monitoring the $^5D_1$ emission of such pairs at 5380 Å. Emission from $^5D_0$, $^5D_1$, and $^5D_2$ levels is observed in the symmetric pairs following $^5D_2$ excitation.

3.3. The Nature of the Cluster Sites. Although the number of bands in the emission and excitation spectra of the clusters probably can be rationalized in terms of an asymmetric pair, the effect of introducing Gd^{3+} on the luminescence properties of the clusters cannot. The overall optical properties of the cluster can be better explained in terms of the cluster consisting of three (or more) strongly coupled lanthanide ions.

The positions and relative intensities of the cluster bands are unaffected by Gd co-doping, but co-doping retards the $^5D_0$ decay constant by a factor greater than 7 at 298 K. This strongly implies that Gd ions are being incorporated into the cluster, and that $^5D_0$ quenching in the Eu-doped samples is due to energy transfer to other ions in the cluster. Since there is no efficient $^5D_0$ quenching process for transfer to one Eu acceptor, at least two Eu acceptors must be present in the clusters. (In fact, it may be more probable that three acceptors are present, since two acceptors would still require a multiphonon-assisted process.) The general importance of many-body processes to energy transfer between trivalent lanthanides has been discussed in the literature[33,34] and has been used to explain the self-quenching of $Eu^{3+}(^5D_0)$ emission in several systems.[35] As discussed in section 3.2, the inability to resolve individual sites within the cluster for the codoped sample also supports a higher-order cluster.

Note also that a multiple-ion cluster would explain the lack of $^5D_2$ or $^5D_1$ emission, even in Gd codoped samples. With one Gd^{3+} incorporated into the cluster, two other Eu ions would remain, and there are numerous possible cross-relaxation pathways out of $^5D_2$ and $^5D_1$ to a single Eu acceptor. Certainly, one would like to test this hypothesis by increasing the Gd-to-Eu ratio in the lattice such that a significant number of clusters exist which contain only one Eu ion.

A higher order cluster in $CsMgCl_3$ would almost certainly require a significant localized disturbance of the native lattice structure. This is supported by the observation that the sharpness of the cluster bands does not increase in low-temperature spectra compared to the symmetric pair bands, indicating significant inhomogeneous broadening for the cluster.

3.4. Energy Levels and Emission Spectra for the Symmetric Pair. Figure 5 shows the major portion of the visible emission spectrum of Eu^{3+} in symmetric Eu−Eu pairs in 0.5% Eu:$CsMgCl_3$ resulting from $^5D_2$ excitation at 10, 77, 125, and 298 K. As discussed in sections 3.5 and 3.7, the temperature dependence of Eu−Eu pair emission is due to the temperature dependence of the $^5D_2 \rightarrow {}^5D_1$, $^5D_0$, and $^5D_1 \rightarrow {}^5D_0$ cross-relaxation processes. Intrinsic $^5D_2 \rightarrow {}^5D_1$, $^5D_0$, and $^5D_1 \rightarrow {}^5D_0$ relaxation via radiative and multiphonon mechanisms is quite inefficient. Therefore, following $^5D_2$ excitation, $^5D_1$ is effectively populated only by $^5D_2 \rightarrow {}^5D_1$ cross relaxation, and $^5D_0$ is populated either by direct $^5D_2 \rightarrow {}^5D_0$ cross relaxation or by a cascade mechanism of sequential $^5D_2 \rightarrow {}^5D_1 \rightarrow {}^5D_0$ cross relaxation.

At 10 K, $^5D_2$ emission accounts for approximately 60% of pair luminescence (in terms of the number of photons emitted

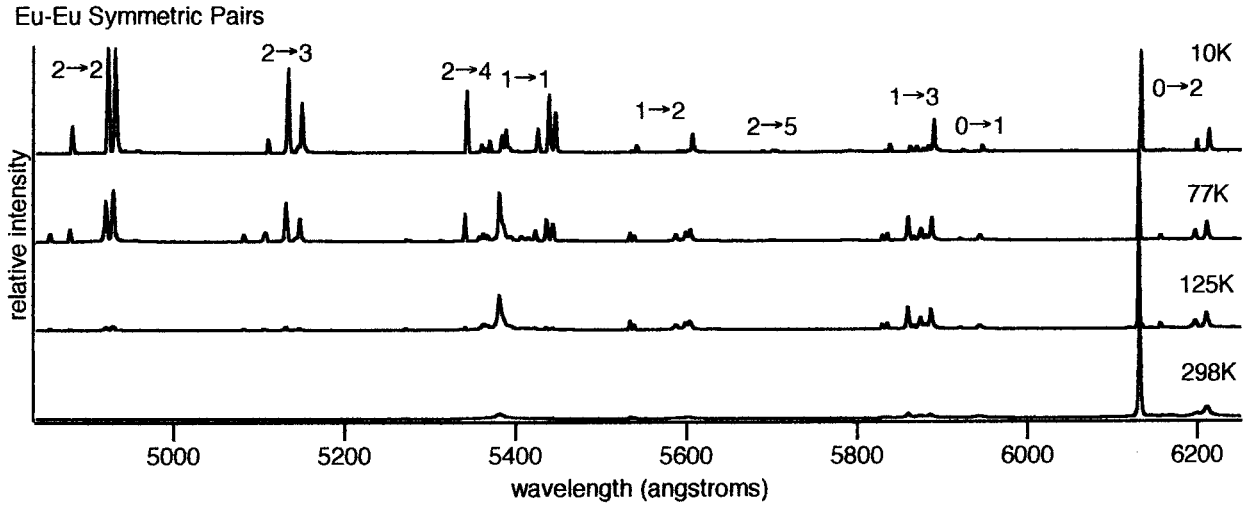

Figure 5. The 10, 77, 125, and 298 K emission spectra of 0.5% Eu:$CsMgCl_3$ obtained by $^5D_2$ excitation of Eu^{3+} in symmetric pairs at 4674 Å. Spectra are corrected for instrument response to photon counts/$d\lambda$.

per time interval) but contributes less than 1% to total emission at 298 K. The decrease in the relative quantum efficiency of $^5D_2$ emission is due almost entirely to an increase in the $^5D_2 \rightarrow {}^5D_1$ cross-relaxation rate. The relative quantum efficiency of $^5D_1$ increases from ~20% at 10 K to a maximum of ~55% at 125 K as a result of $^5D_2 \rightarrow {}^5D_1$ cross relaxation. As the temperature is raised above 125 K, however, the relative quantum efficiency of $^5D_1$ emission decreases due to the increasing efficiency of $^5D_1 \rightarrow {}^5D_0$ cross relaxation, falling to less than 30% at 298 K. Because of the increasing efficiency of sequential $^5D_2 \rightarrow {}^5D_1 \rightarrow {}^5D_0$ cross relaxation, the relative quantum efficiency of $^5D_0$ emission increases with increasing temperature over the entire temperature range, increasing from ~20% of total emission at 10 K to ~70% at 298 K.

We note that excitation into the $^5D_2$ region also results in weak Eu^{2+} emission, which does not appear in Figure 5 because the short-lived Eu^{2+} contribution has been eliminated using time resolution. The appearance of Eu^{2+} emission is, however, due to direct excitation of Eu^{2+} ions, and we find no evidence of any interaction between Eu^{2+} and the symmetric pairs.

The crystal-field energy levels for Eu^{3+} in symmetric pairs in $CsMgCl_3$ are given in Table 1 for 298 and 9 K and are compared to those reported be Pellé et al.[16] for the analogous pairs in $CsCdBr_3$ at 10 K. Overall, the energy-level structure of the symmetric pair is quite similar in the two lattices. Note that the crystal-field levels of the ^5D_J multiplets in $CsMgCl_3$ shift almost uniformly to lower energies as temperature decreases from room temperature to 9 K. We have noted small sample-to-sample variations (≤ 4 cm^{-1}) in the energy levels of Eu^{3+} in the symmetric pairs; all energy levels in Table 1 are those determined for the same 0.5% Eu:$CsMgCl_3$ sample.

Although the energy-level structure of Eu^{3+} in symmetric pairs is similar in $CsMgCl_3$ and $CsCdBr_3$, the luminescence behavior is not. From measurements made in our lab on 0.5% Eu in $CsCdBr_3$, we find that all Eu^{3+} emission is quenched at room temperature and see no evidence of emission from $^5D_1$ or $^5D_2$ at any temperature down to 77K (below which we have made no measurements). Pellé et. al.[16] report $^5D_1$ emission at 10 K, but no $^5D_2$ emission was detected. In contrast, $^5D_0$ relaxation rates in $CsMgCl_3$ are virtually independent of temperature from room temperature to 10 K, and $^5D_1$ and $^5D_2$ emission is easily detectable at room temperature. A possible explanation for the difference in luminescent behavior in the two lattices invokes the presence of a low-lying ligand-to-metal charge transfer state in $CsCdBr_3$, through which Eu^{3+} emission is quenched. Such a state would be at much higher energy in $CsMgCl_3$ and would, therefore, not affect Eu^{3+} emission. We point out that $CsCdBr_3$ doped with 0.5% Eu is bright yellow, while 0.5% Eu:$CsMgCl_3$ is colorless. However, the color difference might be explained in terms of different partitioning of Eu between the Eu^{3+} and Eu^{2+} in the two compounds, and further investigation is required to settle the question.

TABLE 1: Crystal-Field Energy Levels of Eu^{3+} in Symmetric Pairs in $CsMgCl_3$ at 298 K and 9 K (This Work) and in $CsCdBr_3$ at 10 K (from ref 16)[a]

	$CsMgCl_3$		$CsCdBr_3$[16]
multiplet	298 K	9 K	10 K
$^7F_0$	0	0	0 (A_1)
$^7F_1$	317	315	333 (A_2)
	382	380	380 (E)
$^7F_2$	900	892	896 (E)
	1074	1067	1067 (A_1)
	1106	1102	1090 (E)
$^7F_3$	1810	1810	1791 (A_2)
		1897	1877 (A_1)
	1903	1901	1887 (E)
	1946	1943	1928 (A_2)
	1961	1960	1959 (E)
$^7F_4$		2660	2635 (E)
		2721	2688 (A_1)
		2948	2929 (E)
		2990	2972 (E)
			2989 (A_2)
		3015	3003 (A_1)
$^5D_0$	17203	17192	17207 (A_1)
$^5D_1$	18950	18935	18959 (E)
	18966	18953	18972 (A_2)
$^5D_2$	(21387)	21372	
	(21387)	21374	
	21480	21471	

[a] Values given in cm^{-1}. Symmetry assignments for the energy levels in $CsCdBr_3$ are given in parentheses.

3.5. $^5D_1$ Relaxation in Symmetric Pairs. As mentioned in section 3.2, $^5D_1$ decay constants are larger in Eu−Eu pairs compared to Eu−Gd pairs due to cross relaxation between Eu^{3+} ions. In Eu-doped samples, only Eu−Eu pairs are present and observed $^5D_1$ decays are single-exponential. $^5D_1$ decay constants for Eu−Eu pairs were measured as a function of temperature in 0.5% Eu and 0.1% Eu samples, from which very comparable results were obtained. The Eu−Eu decay constants can be

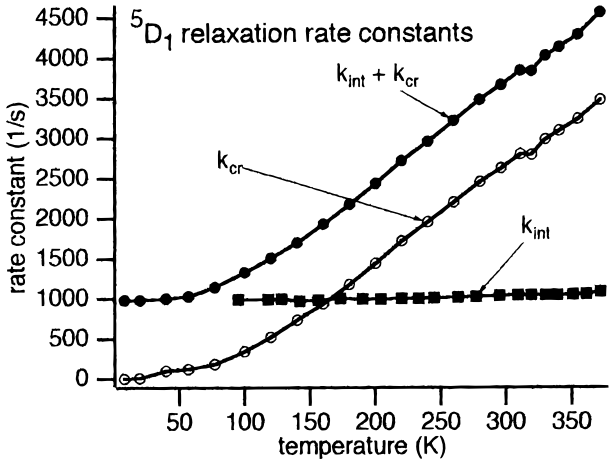

Figure 6. Temperature dependence of $^5D_1$ relaxation constants for Eu^{3+} in symmetric Eu−Eu pairs for total relaxation, $k_{int} + k_{cr}$ (closed circles); cross relaxation, k_{cr} (open circles); and intrinsic relaxation, k_{int} (squares). Refer to section 3.5.

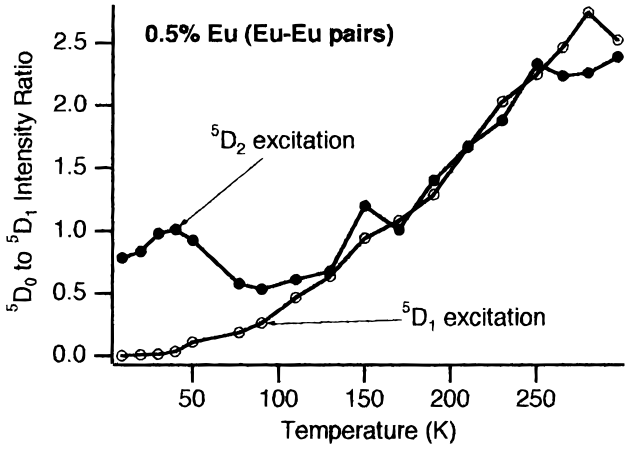

Figure 7. Comparison of the temperature dependence of the intensity ratio of $^5D_0$ to $^5D_1$ emission in symmetric Eu−Eu pairs exciting into $^5D_2$ (closed circles) and $^5D_1$ (open circles). Refer to sections 3.5 and 3.7.

viewed as the sum of the intrinsic decay constants, k_{int}, resulting from single-lanthanide relaxation processes, plus the decay constant due to cross relaxation, k_{cr}.

The intrinsic decay constants, k_{int}, were measured from Eu−Gd pair emission in the 0.5% Eu + 0.5% Gd sample. Since emission from both Eu−Eu and Eu−Gd pairs is observed, the time dependence of $Eu^{3+}(^5D_1)$ emission is given by

$$I(t) = I^{Eu-Gd}(0)e^{-k_{int}t} + I^{Eu-Eu}(0)e^{-(k_{int}+k_{cr})t} \qquad (1)$$

Fits to $^5D_1$ decay curves were achieved by fixing $k_{int} + k_{cr}$ at values determined from the 0.5% Eu sample and treating k_{int}, $I^{Eu-Gd}(0)$, and $I^{Eu-Eu}(0)$ as variable parameters. The cross relaxation constants, k_{cr}, are, therefore, equal to the difference in the total decay constants observed for Eu−Eu and Eu−Gd pairs.

Figure 6 shows the values of $k_{int} + k_{cr}$, k_{cr}, and k_{int} for $^5D_1$ relaxation versus temperature from 10 to 372 K. Reflecting inefficient multiphonon relaxation in this system, the intrinsic relaxation rate is almost temperature independent, dropping from 1083 s^{-1} at 372 K to 980 s^{-1} at 10 K. Intrinsic $^5D_1$ relaxation is probably almost entirely radiative, the slight drop in decay constant values with decreasing temperature being attributed to the loss of vibronic intensity. The cross relaxation rate constant, k_{cr}, shows a nearly linear decrease from 3480 s^{-1} at 372 K to 340 s^{-1} at 100 K, then trails off slowly to near zero at 10 K.

The effect of cross relaxation on the luminescence properties of Eu−Eu pairs using $^5D_1$ excitation is shown in Figure 7, in which the $^5D_0$-to-$^5D_1$ intensity ratio is plotted vs temperature from 10 to 298 K. The ratio corresponds to the relative number of photons emitted from the $^5D_0$ and $^5D_1$ levels. This plot was generated using uncorrected emission spectra of the $^5D_0 \rightarrow {}^7F_2$ and $^5D_1 \rightarrow {}^7F_2$ regions, scaling their ratios by a constant such that the room-temperature value equals k_{cr}/k_{int} (see Figure 6). Scaling the data in this way assumes that the intrinsic quantum efficiencies of $^5D_0$ and $^5D_1$ emission are similar (neglecting cross relaxation) and that intrinsic $^5D_1 \rightarrow {}^5D_0$ relaxation is negligible compared to k_{cr} at room temperature. In fact, after scaling to the room-temperature datum, the $^5D_0$-to-$^5D_1$ intensity ratio is within experimental error of k_{cr}/k_{int} (from Figure 6) over the entire temperature range, indicating that intrinsic $^5D_1 \rightarrow {}^5D_0$ relaxation can be neglected entirely and that $^5D_0$ is fed only via cross relaxation processes. Note that, at 10 K, both k_{cr} and the $^5D_0$-to-$^5D_1$ ratio are approximately zero and essentially all emission is out of $^5D_1$ to ^7F_J. That intrinsic $^5D_1 \rightarrow {}^5D_0$ relaxation is negligible is further supported by our ability to describe the time dependence of $^5D_0$ emission following $^5D_1$ excitation in the 0.5% Eu + 0.5% Gd sample completely in terms of Eu−Eu pairs, showing that Eu−Gd pairs do not contribute to $^5D_0$ emission.

3.6. Partitioning of Eu between Eu^{2+} and Eu^{3+}. Using the $^5D_1$ decay data and the nominal lanthanide concentrations for the 0.5% Eu + 0.5% Gd sample, it is possible to make a crude estimate as to how Eu partitions itself between the two oxidation states. Fits of the $^5D_1$ decay curves following direct $^5D_1$ excitation using eq 1 yields an average value of $I^{Eu-Gd}(0)/I^{Eu-Eu}(0) = 1.55 \pm 0.08$, which, in turn, implies that the ratio of Gd^{3+} to Eu^{3+} in symmetric pairs is 1.55. The nominal ratio of the total concentration of Gd to Eu is 1. To achieve an actual Gd^{3+} to Eu^{3+} ratio of 1.55 would require 64% of Eu to remain as Eu^{3+}.

Since the actual Eu and Gd concentrations in the crystal are not known, this calculated percentage is of little quantitative value, but does indicate that a significant percentage of Eu exists in the lattice as Eu^{3+}.

3.7. $^5D_2$ Relaxation in Symmetric Pairs. Efficient cross relaxation of the $^5D_2$ levels in Eu−Eu pairs is also observed. From $^5D_2$ emission decay curves for the Eu-doped and Eu−Gd co-doped samples, the intrinsic decay constants, k_{int}, and cross relaxation decay constants, k_{cr}, were determined from 10 to 298 K in a manner analogous to that described in section 3.5 for $^5D_1$ cross relaxation. The temperature dependence of k_{cr} for $^5D_2$ relaxation is shown in Figure 8. The inset in Figure 8 also shows the breakdown of the total decay constant, $k_{cr} + k_{int}$, and the intrinsic decay constant, k_{int}, for temperatures below 90 K.

The intrinsic decay constant, k_{int}, is relatively insensitive to temperature and shows similar behavior to that observed for $^5D_1$ (see section 3.5), dropping from 1090 s^{-1} at 298 K to 840 s^{-1} at 10 K.

The cross relaxation decay constant, k_{cr}, is very sensitive to temperature between 77 K ($k_{cr} = 1590$ s^{-1}) and 298 K ($k_{cr} = 1.28 \times 10^5$ s^{-1}). Below 77 K, k_{cr} becomes relatively stable, dropping only from 640 s^{-1} at 50 K to 535 s^{-1} at 10 K. Note that the behavior of cross relaxation out of $^5D_2$ differs quite markedly from that out of $^5D_1$; it is more strongly temperature dependent and is much more efficient over the entire temperature region.

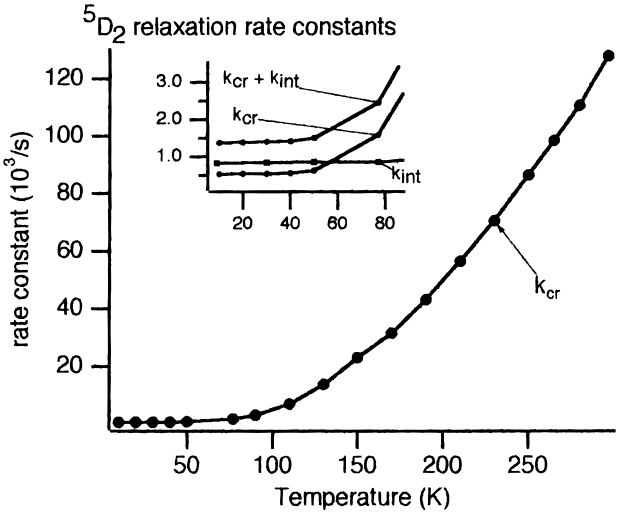

Figure 8. Temperature dependence of the rate constant for cross relaxation, k_{cr}, out of $^5D_2$ in symmetric Eu−Eu pairs. The inset shows the breakdown of the total decay constant, $k_{cr} + k_{int}$, and the intrinsic decay constant, k_{int}, for temperatures below 90 K. Refer to section 3.7.

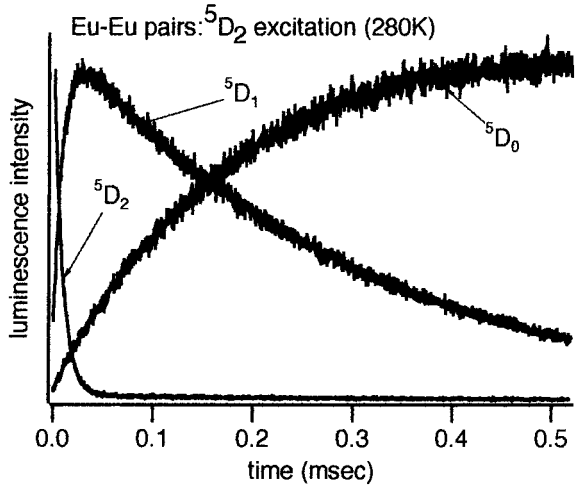

Figure 9. Time dependence of $^5D_2$, $^5D_1$, and $^5D_0$ emission from symmetric Eu−Eu pairs following $^5D_2$ excitation in 0.5% Eu:$CsMgCl_3$ at 280 K.

Cross relaxation out of $^5D_2$ results in the immediate population of $^5D_1$ and/or $^5D_0$. Figure 7 shows the $^5D_0$-to-$^5D_1$ intensity ratios in Eu−Eu pairs as a function of temperature comparing $^5D_1$ and $^5D_2$ excitation. The intensity ratios for $^5D_2$ excitation are scaled with the same constant used for $^5D_1$ excitation (see section 3.5). Between 298 and 130 K, the observed intensity ratios match closely for $^5D_1$ and $^5D_2$ excitation, indicating that cross relaxation is dominated by relaxation to $^5D_1$. Below 130 K, the $^5D_0$-to-$^5D_1$ intensity ratio is higher for $^5D_2$ excitation, indicating significant direct feeding of $^5D_0$ from $^5D_2$. As discussed later in this section, we attribute essentially all of this direct feeding to cross relaxation processes, since intrinsic $^5D_2 \rightarrow {}^5D_0$ relaxation appears to be negligible.

The dynamics of $^5D_2$ relaxation in Eu−Eu pairs at higher temperatures readily become apparent when comparing the time dependence of $^5D_2$, $^5D_1$, and $^5D_0$ luminescence following $^5D_2$ excitation, as is shown for the 0.5% Eu sample at 280 K in Figure 9. The rise of $^5D_1$ emission matches the fast $^5D_2$ decay, consistent with feeding from $^5D_2$. In contrast, there is obviously no significant fast rise component in $^5D_0$ emission to indicate direct feeding from $^5D_2$. Instead, the slow $^5D_0$ rise is consistent with cascade relaxation from $^5D_2$ through $^5D_1$.

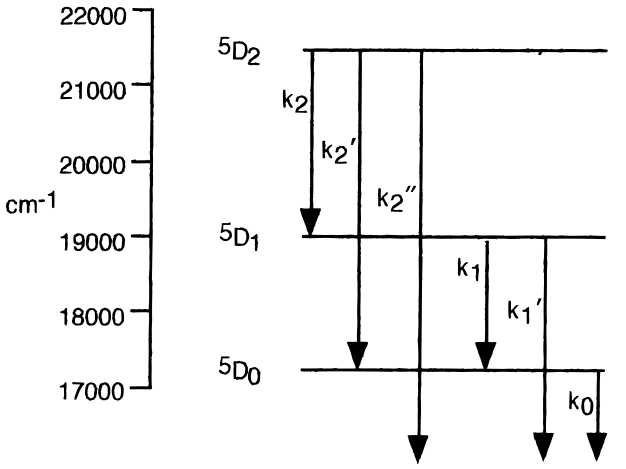

Figure 10. Schematic representation of the relaxation pathways out of the ^5D_J ($J = 0-2$) states of Eu^{3+} in symmetric pairs. Labels refer to the rate constants used in eqs 2−4 and 6 in section 3.7.

In general, the time dependence of $^5D_0$ luminescence following $^5D_2$ excitation in Eu−Eu pairs is given by

$$I(t) = K_1[(k_0 - k_1 - k_1')^{-1}(e^{-k_0 t} - e^{-(k_1+k_1')t}) + (k_0 - k_2 - k_2' - k_2'')^{-1}(e^{-(k_2+k_2'+k_2'')t} - e^{-k_0 t})] + K_2[e^{-(k_2+k_2'+k_2'')t} - e^{-k_0 t}] \quad (2)$$

where $K_1 = k_1 k_2[^5D_2]_0(k_1 + k_1' - k_2 - k_2' - k_2'')^{-1}$, $K_2 = k_2'[^5D_2]_0(k_0 - k_2 - k_2' - k_2'')^{-1}$, and all decay constants correspond to the pathways illustrated in Figure 10. The term in eq 2 with K_1 as a coefficient describes luminescence due to cascade feeding via $^5D_1$, whereas the K_2 term describes direct population of $^5D_0$ from $^5D_2$. K_1 and K_2 can be viewed as scaling factors for the indirect and direct feeding pathways, respectively. Equation 2 was used to fit the observed time dependence of $^5D_0$ emission following $^5D_2$ excitation in the 0.1% Eu and 0.5% Eu samples using K_1 and K_2 as the only adjustable parameters. All other rate constants were fixed at values determined from the decay curves of ^5D_J ($J = 0-2$) using direct excitation into the multiplet of interest; k_0 is the $^5D_0$ decay constant, $(k_1 + k_1')$ is the $^5D_1$ decay constant, and $(k_2 + k_2' + k_2'')$ is the $^5D_2$ decay constant.

At temperatures of 130 K or greater, good fits of eq 2 to $^5D_0$ emission are obtained even when omitting the direct feeding mechanism (i.e., setting $K_2 = 0$), which is in agreement with our earlier statement that direct feeding is unimportant at higher temperatures. The intensity data in Figure 7 indicate that direct feeding begins to compete with indirect processes below 130 K; this conclusion is supported by the time dependence of $^5D_0$ emission. Figure 11 shows the results of fitting eq 2 to $^5D_0$ emission following $^5D_2$ excitation in the 0.5% Eu sample at 90 K. The results of the fit are broken down into separate contributions from direct and indirect feeding, showing significant feeding from both mechanisms. At 90 K, we estimate ~47% of $^5D_0$ emission is due to direct feeding. At 10 K, essentially all $^5D_0$ emission is due to direct feeding from $^5D_2$, not because the $^5D_2 \rightarrow {}^5D_1$ pathway is inactive (as discussed below), but because population of $^5D_1$ no longer results in $^5D_0$ emission (see section 3.5).

Measurements of the time dependence of $^5D_1$ and $^5D_0$ emission following $^5D_2$ excitation in the 0.5% Eu + 0.5% Gd sample show no significant contribution from Eu−Gd pairs at any temperature. This implies that k_2 and k_2' in Eu−Eu pairs are always much larger than in Eu−Gd pairs and that contribu-

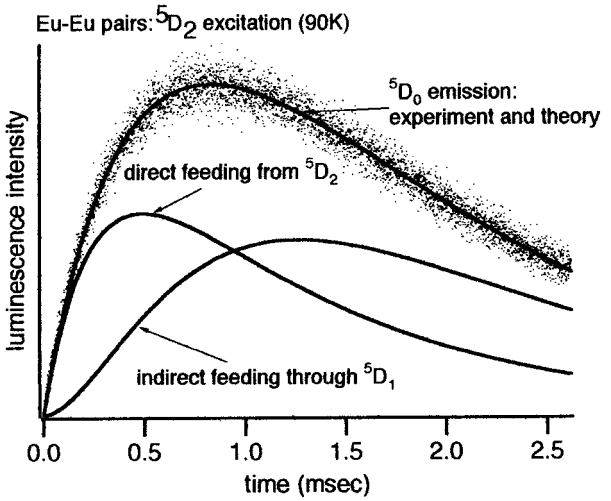

Figure 11. Fit of eq 2 (upper solid line) to the observed time dependence of $^5D_0$ emission (6131.7 Å) from symmetric Eu−Eu pairs in 0.5% Eu:$CsMgCl_3$ at 90 K following $^5D_2$ excitation at 4673 Å (dots). The two lower solid lines show the contributions of indirect feeding of $^5D_0$ from $^5D_2$ via $^5D_1$ (corresponding to the first term in eq 2) and of direct feeding of $^5D_0$ from $^5D_2$ (corresponding to the second term in eq 2) to the overall fit. Refer to section 3.7.

tions to k_2 and k_2' from intrinsic relaxation processes can be ignored for Eu−Eu pairs. This allows us to assign $k_2 + k_2' = k_{cr}$ in Eu−Eu pairs, which will be used below to determine the absolute values for the two cross relaxation decay constants, k_2 and k_2'.

The ratios of K_1 to K_2 obtained from fits to eq 2 can be used to estimate how cross relaxation out of $^5D_2$ branches between $^5D_1$ and $^5D_0$. The ratio of the rate constants for $^5D_2 \rightarrow {}^5D_1$ to $^5D_2 \rightarrow {}^5D_0$ relaxation is given by k_2/k_2' (refer to Figure 10), which is related to K_1/K_2 by

$$\frac{k_2}{k_2'} = \frac{K_1}{K_2}\frac{k_1 + k_1' - k_2 - k_2' - k_2''}{k_1(k_0 - k_2 - k_2' - k_2'')} \tag{3}$$

where k_1 is the rate constant for $^5D_1$ cross relaxation, k_0 is the $^5D_0$ decay constant, $(k_1 + k_1')$ is the $^5D_1$ decay constant, and $(k_2 + k_2' + k_2'')$ is the $^5D_2$ decay constant. Using eq 3, values for k_2/k_2' at 77, 90, and 110 K are 3.3, 5.7, and 9.7, respectively, reflecting the growing dominance of $^5D_2 \rightarrow {}^5D_1$ relaxation, k_2, with increasing temperature.

The k_2/k_2' ratios, and, therefore, k_2 and k_2', can be determined over a broader temperature range using the $^5D_0$-to-$^5D_1$ intensity ratio data in Figure 7, the $^5D_1$ relaxation constants in Figure 6, and the following relation:

$$\frac{k_2}{k_2'} = \frac{k_1 + k_1'}{I_R k_1' - k_1} \tag{4}$$

where I_R is the $^5D_0$-to-$^5D_1$ intensity ratio using $^5D_2$ excitation, $k_1 + k_1'$ is the rate constant for $^5D_1$ relaxation in Eu−Eu pairs, k_1 is the rate constant for cross relaxation out of $^5D_1$, and k_1' is the rate constant for $^5D_1$ relaxation in Eu−Gd pairs. The absolute values of the $^5D_2 \rightarrow {}^5D_1$ and $^5D_2 \rightarrow {}^5D_0$ cross relaxation constants can then be determined using $k_2 + k_2' = k_{cr}$, where k_{cr} are the $^5D_2$ cross relaxation constants given in Figure 8. Values for k_2 and k_2' determined in this manner are plotted vs temperature in Figure 12 from 10 to 90 K. At 10 K, $^5D_2 \rightarrow {}^5D_1$ and $^5D_2 \rightarrow {}^5D_0$ cross relaxation have similar rate constants. However, $^5D_2 \rightarrow {}^5D_1$ cross relaxation shows a much stronger temperature dependence than does $^5D_2 \rightarrow {}^5D_0$ cross relaxation

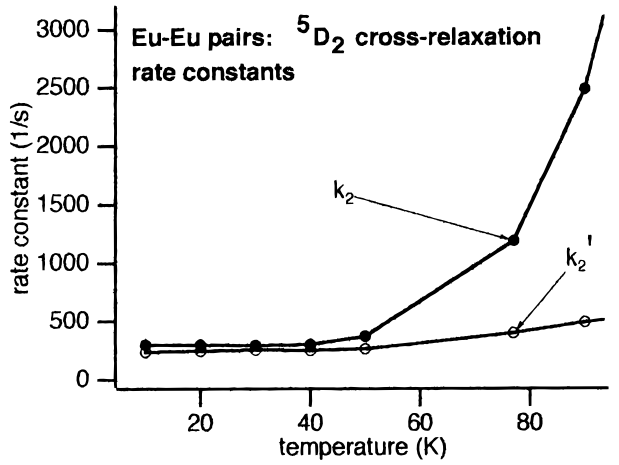

Figure 12. Temperature dependence of rate constants for $^5D_2 \rightarrow {}^5D_1$ (k_2) and $^5D_2 \rightarrow {}^5D_0$ (k_2') cross relaxation in symmetric Eu−Eu pairs. Refer to section 3.7.

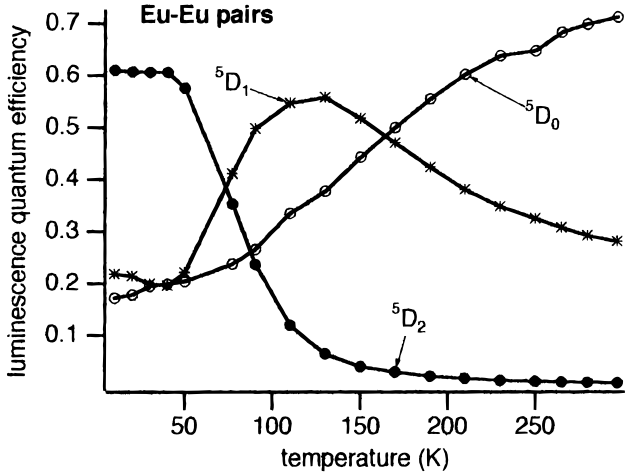

Figure 13. Temperature dependence of luminescence quantum efficiencies of $^5D_2$, $^5D_1$, and $^5D_0$ emission from symmetric Eu−Eu pairs following $^5D_2$ excitation. Refer to section 3.7.

and quickly dominates the overall cross-relaxation process as temperature is increased.

The luminescence properties of symmetrical Eu−Eu pairs upon $^5D_2$ excitation are conveniently summarized in Figure 13, which shows the quantum efficiencies of $^5D_2$, $^5D_1$, and $^5D_0$ emission as a function of temperature. The quantum efficiency of $^5D_2$ emission, $\eta(^5D_2)$, was calculated using

$$\eta(^5D_2) = \frac{k_{int}}{k_{int} + k_{cr}} \tag{5}$$

where k_{int} is the $^5D_2$ decay constant in Eu−Gd pairs and $(k_{int} + k_{cr})$ is the $^5D_2$ decay constant in Eu−Eu pairs (see Figure 8). The quantum efficiency of $^5D_1$ emission, $\eta(^5D_1)$, was calculated using

$$\eta(^5D_1) = \frac{k_2}{k_{int}(^5D_2) + k_{cr}(^5D_2)}\frac{k_{int}(^5D_1)}{k_{int}(^5D_1) + k_{cr}(^5D_1)} \tag{6}$$

where k_2 is the $^5D_2 \rightarrow {}^5D_1$ decay constant (see Figures 10 and 12), $k_{int}(^5D_2) + k_{cr}(^5D_2)$ is the $^5D_2$ decay constant in Eu−Eu pairs (see Figure 8), $k_{int}(^5D_1)$ is the $^5D_1$ decay constant in Eu−Gd pairs, and $k_{int}(^5D_1) + k_{cr}(^5D_1)$ is the $^5D_1$ decay constant in Eu−Eu pairs (see Figure 6). At temperatures up to 110 K, k_2

values were calculated as described for Figure 12. Above 110 K, we used the approximation $k_2 \cong k_{cr}(^5D_2)$, since, as discussed previously, $^5D_2 \rightarrow {}^5D_1$ cross relaxation is dominant in this temperature range. The quantum efficiency of $^5D_0$ emission, $\eta(^5D_0)$, was calculated using

$$\eta(^5D_0) = 1-\eta(^5D_1)-\eta(^5D_2) \quad (7)$$

Equations 5−7 assume that intrinsic relaxation from $^5D_2$, $^5D_1$, and $^5D_0$ is predominately radiative.

Up to 50 K, the quantum efficiency of $^5D_2$ is ∼0.6 but drops dramatically with further increase in temperature due to cross relaxation quenching. From 10 to 130 K, the quantum efficiency of $^5D_1$ increases with increasing temperature to a maximum of ∼0.55. The increase of $\eta(^5D_1)$ over this temperature range is due to the fact that the feeding rate of $^5D_1$ via $^5D_2 \rightarrow {}^5D_1$ cross relaxation is increasing more rapidly than is quenching via cross relaxation out of $^5D_1$. Above 130 K, $\eta(^5D_1)$ decreases with increasing temperature as the quenching due to cross relaxation out of $^5D_1$ begins to dominate. The quantum efficiency of $^5D_0$ increases with temperature over the entire temperature range, due mainly to the increasing efficiency by which it is fed through $^5D_1$.

4. Conclusions

Eu-doped $CsMgCl_3$ crystals grown from melts of $CsMgCl_3$ and anhydrous $EuCl_3$ under vacuum via the Bridgman method exhibit broad-band Eu^{2+} emission and sharp-line Eu^{3+} emission, both of which are efficient. The precise partitioning of Eu between the trivalent and divalent state was not determined, but a significant percentage of Eu ions appear to remain in the trivalent state. Luminescence is observed from Eu^{3+} ions in symmetric pairs and in what are probably clusters containing three or more lanthanide ions. The clusters are not seen in samples with low concentrations (0.1 mol %) of europium.

$^5D_2$ and $^5D_1$ emission from Eu^{3+} in clusters is strongly quenched in Eu-doped and in Eu−Gd codoped samples at room temperature. $^5D_0$ emission is partially quenched in Eu-doped samples at room temperature, but not in Eu−Gd codoped samples. The influence of Gd codoping on $^5D_0$ emission and lack thereof on $^5D_1$ and $^5D_2$ emission is consistent with a many-body process for $^5D_0$ quenching and a two-ion process for $^5D_1$ and $^5D_2$ quenching. We offer no suggestions as to the structure of the cluster, but note that it must involve a significant disruption of the native lattice. This is supported by the fact that we do not observe substantial sharpening of lines in the cluster spectra at lower temperatures (in contrast to significant sharpening of the symmetric pair lines), indicating large inhomogeneities in the cluster.

Eu^{3+} in symmetric pairs exhibits emission from $^5D_0$, $^5D_1$, and $^5D_2$. Temperature-dependent quenching of $^5D_1$ and $^5D_2$ luminescence is observed in Eu−Eu pairs, but not Eu−Gd pairs, and is attributed to cross relaxation between Eu^{3+} ions within the pair. Rate constants for cross relaxation out of $^5D_1$ and $^5D_2$ are given as a function of temperature. Up to 50 K, cross relaxation out of $^5D_2$ partitions approximately equally between $^5D_2 \rightarrow {}^5D_1$ and $^5D_2 \rightarrow {}^5D_0$, but the $^5D_2 \rightarrow {}^5D_1$ process quickly becomes dominant as temperature is increased.

It is interesting to compare the optical properties of Eu-doped $CsMgCl_3$ to those of Eu-doped $CsCdBr_3$. In both systems, Eu is stabilized in the divalent and trivalent state, although the divalent state is reported to dominate in $CsCdBr_3$. The energy level structure of Eu^{2+} appears similar in both systems, yet Eu^{2+} emission is more efficient in $CsMgCl_3$. Similarly, the energy level structure of Eu^{3+} ions in symmetric pairs in $CsMgCl_3$ is quite similar to that reported for the analogous pairs in $CsCdBr_3$, but the luminescence behavior is quite different. Emission from $^5D_2$ and $^5D_1$ is much more strongly quenched in $CsCdBr_3$, and $^5D_0$ emission also exhibits temperature-dependent quenching. A possible explanation for the difference in luminescent behavior of Eu^{3+} symmetric pairs in the two lattices is the presence of a low-lying ligand-to-metal charge transfer state in $CsCdBr_3$, through which the ^5D_J ($J = 0-2$) states could be quenched.

The rate constants for Eu−Eu cross relaxation presented here will be used in a future study to analyze the mechanisms responsible for energy transfer in this system.

Acknowledgment. Acknowledgment is made to the donors of the Petroleum Research Fund, administered by the ACS, for partial support of this research (ACS-PRF 32365-B6). Additional support was provided by a grant to P. S. May from DoD (Grant DAAG55-98-1-0264).

References and Notes

(1) McPherson, G. L.; Henling, L. M. *Phys. Rev. B* **1977**, *16*, 1889.
(2) Henling, L. M.; McPherson, G. L. *Phys. Rev. B* **1977**, *16*, 4756.
(3) Antic-Fidancev, E.; Lemaitre-Blaise, M.; Chaminade, J. P.; Porcher, P. *J. Alloys. Compd.* **1995**, *225*, 95.
(4) Neukum, J.; Bodenschatz, N.; Heber, J. *Phys. Rev. B* **1994**, *50*, 3536.
(5) Schaefer, U.; Neukum, J.; Bodenschatz, N.; Heber, J. *J. Lumin.* **1994**, *60−61*, 633.
(6) Heber, J.; Schaefer, U.; Neukum, J.; Bodenschatz, N. *Acta Phys. Pol., A* **1993**, *84*, 889.
(7) Barthem, R. B.; Buisson, R.; Cone, R. L. *J. Chem. Phys.* **1989**, *91*, 627.
(8) Barthou, C.; Barthem, R. B. *J. Lumin.* **1990**, *46*, 9.
(9) Barthem, R. B.; Buisson, R.; Madeore, F.; Vial, J. C.; Chaminade, J. P. *J. Phys.* **1987**, *48*, 379.
(10) Barthem, R. B.; Buisson, R.; Vial, J. C.; Chaminade, J. P. *J. Phys., Colloq.* **1985**, *C7*, 113.
(11) Lammers, M. J. J.; Blasse, G. *Chem. Phys. Lett.* **1986**, *126*, 405.
(12) Berdowski, P. A. M.; Lammers, M. J. J.; Blasse, G. *J. Chem. Phys.* **1985**, *83*, 476.
(13) May, P. S.; Sommer, K. D. *J. Phys. Chem. A* **1997**, *101*, 9571.
(14) Mujajii, M.; Jones, G. D.; Syme, R. W. G. *Phys. Rev. B* **1993**, *48*, 710.
(15) Mujaji, M.; Jones, G. D.; Syme, R. W. G. *J. Lumin.* **1992**, *53*, 473.
(16) Pelle, F.; Gardant, N.; Genotelle, M.; Goldner, Ph.; Porcher, P. *J. Phys. Chem. Solids* **1995**, *56*, 1003.
(17) Quagliano, J. R.; Cockroft, N. J.; Gunde, K. E.; Richardson, F. S. *J. Chem. Phys.* **1996**, *105*, 9812.
(18) Pelle, F.; Goldner, Ph. *Opt. Mater.* **1994**, *4*, 121.
(19) Bordallo, H. N.; Barthem, R. B.; Barthou, C. *Solid State Commun.* **1994**, *92*, 721.
(20) Pelle, F.; Goldner, Ph. *Phys. Rev. B* **1993**, *48*, 9995.
(21) McPherson, G. L.; Gharavi, A.; Meyerson, S. L. *Chem. Phys.* **1992**, *165*, 361.
(22) Cockroft, N. J.; Jones, G. D.; Nguyen, D. C. *Phys. Rev. B* **1992**, *45*, 5187.
(23) McPherson, G. L.; Meyerson, S. L. *Chem. Phys. Lett.* **1991**, *179*, 325.
(24) McPherson, G. L.; Meyerson, S. L. *Chem. Phys. Lett.* **1990**, *167*, 471.
(25) Gharavi, A.; McPherson, G. L. *Chem. Phys. Lett.* **1992**, *200*, 279.
(26) Blasse, G.; Wolfert, A.; McPherson, G. L. *J. Solid State Chem.* **1985**, *57*, 396.
(27) Murdoch, K. M.; Cockroft, N. J. *Phys. Rev. B* **1996**, *54*, 4589.
(28) Bodenschatz, N.; Neukum, J.; Heber, J. *J. Lumin.* **1995**, *66−67*, 213.
(29) Goldner, Ph.; Pelle, F. *J. Lumin.* **1994**, *60−61*, 651.
(30) Gharavi, A.; McPherson, G. L. *J. Opt. Soc. Am. B* **1994**, *11*, 913.
(31) McPherson, A. M.; McPherson, G. L. *Solid State Commun.* **1981**, *37*, 501.
(32) Both samples were synthesized in our lab.
(33) Fong, F. K.; Diestler, D. J. *J. Chem. Phys.* **1972**, *56*, 2875.
(34) Grant, W. J. C. *Phys. Rev. B* **1971**, *4*, 648.
(35) See, for example: Van Uitert, L. G.; Johnson, L. F. *J. Chem. Phys.* **1966**, *44*, 3514. Ke, H. D.; Birnbaum, E. R. *J. Lumin.* **1995**, *63*, 9.